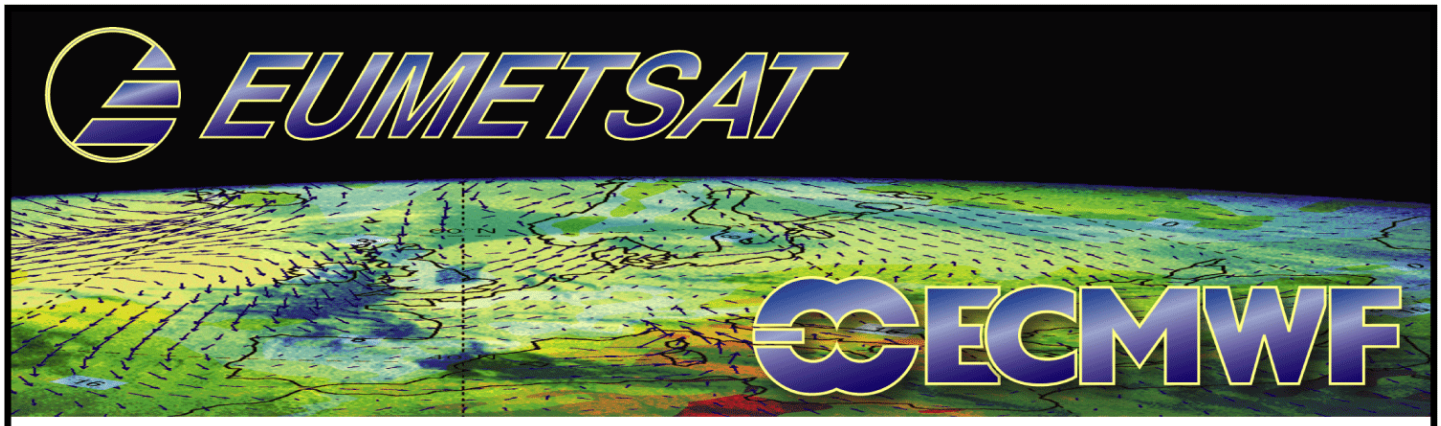

EUMETSAT / ECMWF Fellowship Programme
Research Report No. 16

Assimilating GPS radio occultation measurements with two-dimensional bending angle observation operators

S.B. Healy, J.R. Eyre, M. Hamrud
and Jean-Noël Thépaut

August 2006

Series: EUMETSAT/ECMWF Fellowship Programme Research Reports

A full list of ECMWF Publications can be found on our web site under:
http://www.ecmwf.int/publications/

Contact: library@ecmwf.int

European Centre for Medium Range Weather Forecasts
Shinfield Park, Reading, RG2 9AX, England

Abstract

Four-dimensional variational (4D-Var) assimilation forecast impact experiments have been conducted with CHAMP radio occultation measurements from 1st June – 31st July, 2004. The CHAMP bending angles have been assimilated with one-dimensional (1D) and two-dimensional (2D) bending angle observation operators, enabling the potential benefits of the latter to be investigated. Two computationally affordable 2D bending angle observation operators have been considered. The first can be viewed as a straightforward generalisation of the 1D operator. The second is based on a 4th order Runge-Kutta solution of the differential equations defining the ray-path through the refracting atmosphere.

It is demonstrated that the computational cost of the 2D bending angle operators is not prohibitive and that they improve the root-mean-square of the observed minus background (O-B) bending angle departures by around 5% in the lower-troposphere of the northern and southern hemispheres. The O-B distributions in the tropical lower-troposphere are biased low, but the first-guess departure quality control procedure removes $\sim 2 - 3\%$ of the observations and this reduces the bias by around 20%. The assimilation of the CHAMP measurements with both the 1D and 2D operators improves the analysis and forecast fit to radiosonde temperature measurements in the southern hemisphere on the 300, 200, 100 and 50 hPa levels, over the day-1 to day-5 forecast range. The forecast scores in the lower-troposphere for geopotential height and relative humidity are generally neutral, but there is a small improvement in the anomaly correlation of the 500 hPa geopotential height field in the southern hemisphere, over the day-1 to day-2 forecast range. However, there are no clear, statistically significant differences between the 1D and 2D experiments for this two month period.

1 Introduction

From 2006 the GRAS instrument on METOP (Loiselet *et al.* 2000) and the constellation of six satellites, COSMIC (Anthes *et al.* 2000), will provide GPS radio occultation (GPSRO) measurements in near-real-time, for assimilation into operational numerical weather prediction (NWP) systems. The GPS/MET (Kursinski *et al.* 1996; Rocken *et al.* 1997) and CHAMP (Wickert *et al.* 2001) GPSRO experiments have demonstrated that the measurement technique provides temperature information with a sub-Kelvin accuracy between heights of ~ 7 km to 25 km. The measurements are globally distributed, have an all weather capability and good vertical resolution (e.g., Kursinski *et al.* 1997). Theoretical studies have shown that GPSRO measurements and radiances from advanced infrared sounders provide complementary temperature information (Collard and Healy, 2003). Furthermore, recent forecast impact experiments assimilating CHAMP measurements with relatively simple one-dimensional (1D) observation operators at the Met Office (Healy *et al.* 2005) and ECMWF (Healy and Thépaut, 2006) have demonstrated that GPSRO measurements can improve the analysis and forecast fit to radiosonde temperature measurements in the lower-stratosphere. These results are encouraging because they have been achieved with a very small number of GPSRO observations, when compared with the number of conventional and satellite measurements that are already assimilated at the operational centres.

The GPSRO measurements could potentially provide limb-averaged water-vapour information in the lower-troposphere, but it is likely that more sophisticated observation processing and assimilation methods will have to be developed before this information can be exploited effectively in operational NWP. For example, a current area of active research is the implementation of open-loop tracking (Sokolovskiy, 2001), primarily because it should improve the quality of lower-tropospheric measurements. In addition, a number of two-dimensional (2D) GPSRO observation operators have been proposed recently (see section 2) with the aim of reducing forward model errors in the lower-troposphere. In this context, we have investigated the assimilation of GPSRO measurements with 2D bending angle observation operators.

This study represents a continuation of the work presented by Healy and Thépaut (2006) (Referred to as HT06 hereafter). We have performed four-dimensional variational (4D-Var) forecast impact experiments, assimilating CHAMP measurements with both 1D and 2D bending angle observation operators. Two computationally efficient 2D bending angle operators have been developed and used in forecast impact experiments with two months of CHAMP data from June – July, 2004. In section 2, research on the development of 2D (or "non-local") operators is briefly reviewed, and in section 3 we describe the 2D bending angle operators used in this study. The forecast impact experiments using the 4D-Var assimilation system are presented in section 4 and the discussion and conclusions are given in section 5.

2 A review of 2D GPSRO operator research

Before outlining recent work on 2D operators for GPSRO, it is useful to provide some details of the preprocessing of the assimilated quantities – usually either bending angle or refractivity – for the clarity of this section. More detailed descriptions of the basic physics and processing of the measurements are given by Melbourne *et al.* (1994) and Kursinski *et al.* (1997). The measurement geometry is shown in Fig. 1. The path of a radio signal propagating between a GPS satellite and a receiver on a low earth orbiting (LEO) satellite is bent as a result of refractive index gradients in the atmosphere and ionosphere. The ionospheric bending can be removed with standard methods (Vorob'ev and Krasil'nikova, 1994), and it will not be discussed further. The radio signal measured at the LEO is Doppler shifted because of the motion of the satellites, but the Doppler shift is modified because of the bending of the ray-path, which is characterised by a bending angle, α. Deriving α from the Doppler shift is an ill-posed problem. It is made well-posed by assuming *a priori* that the variable known as the impact parameter, a, has the same value at the GPS and LEO satellites. This enables α and a to be derived simultaneously, given accurate estimates of position and velocity of the satellites (Kursinski *et al.* 1997). Physically, the impact parameter, a, is analogous to the angular momentum of a classical particle and it is defined at any point on the ray-path as

$$a = nr\sin\phi \tag{1}$$

where n is the refractive index, r is the radius and ϕ is the angle between the ray vector and the local radius vector (See Fig. 1). The impact parameter value is constant along the ray-path if the refractive index field is spherically symmetric, and when this is the case, a profile of refractive index, n, as a function of height can be derived from the profile of bending angle as function of impact parameter, $\alpha(a)$, using an Abel transform (Kursinski *et al.* 1997).

Eyre (1994) considered the possible strategies for assimilating GPSRO measurements and proposed a computationally inexpensive 2D forward model for the assimilation of bending angle, α, as a function of impact parameter, a. The forward model starts the bending angle calculation at the assumed horizontal location of the tangent point, rather than one of the satellites, and uses the derived impact parameter, a, to determine the ray tangent height. A 1D operator is used initially to estimate the ray-path – in polar co-ordinates (r and θ) – through the 2D occultation plane. The bending angle associated with this ray-path through the 2D plane is then evaluated. Palmer (1998) used this model to investigate the differences of bending angles calculated with 1D and 2D operators and found that the largest differences occurred in cases where the second derivative of the horizontal refractivity ($N = 10^{-6}(n-1)$) gradient was large (See also page 61 Melbourne *et al.* 1994). However, the forward model errors can be much larger than the 1D minus 2D differences when the derived impact parameter, a, is used to determine the ray tangent height in both the 1D and 2D models, because this simplification implicitly assumes that a is constant along the ray-path (Healy 2001). Note that the preprocessing of the measurements from Doppler shift to bending angle is based on the weaker assumption that a has the same value at the GPS and LEO satellites, only requiring that the 2D refractivity gradients have reflection symmetry about the tangent point.

Liu and Zou (2003) distinguished between the geometrical bending angle derived directly from the angle between the ray vectors at the satellites and the bending angle value derived from the Doppler shift, assuming that the impact parameter has the same value at the GPS and LEO. The latter is sometimes called the "pseudo bending angle". They outlined an observation operator for assimilating pseudo bending angle, that initially simulates the Doppler shift and then inverts the Doppler value to determine the pseudo bending angle. Formally, this is reproducing the processing of the observations more closely, and therefore it should reduce the forward modelling errors. However, Liu and Zou (2003) introduced a number of simplifying assumptions when evaluating the Doppler shift, such as starting the ray integration from the assumed tangent point and not requiring the ray-path to intersect the satellites. As a consequence of these assumptions, and the forward model errors caused by the use of a relatively coarse NWP model (See Eq. 2.17 Cohn 1997), they were unable to find any significant differences between pseudo and conventional bending angles. The 2D operator was used in forecast impact experiments (Zou *et al.* 2004), but they did not use the latest observation data sets, and in general their forecast scores were poorer than would be expected at an operational centre.

Poli and Joiner (2004) and Poli (2004) investigated a bending angle model similar to that described by Eyre (1994), and demonstrated that using a 2D operator can reduce the standard deviation of the observation minus simulated values by $\sim$ 10%, for tangent points around 18 km. However, in general their bending angle error estimates in the lower-troposphere appear quite low, because they did not consider the errors associated with use of the impact parameter, a, to determine the ray tangent height to be a forward model error [1].

Syndergaard *et al.* (2005) recently presented a "non-local" (i.e., 2D) refractivity operator. The approach is motivated by the suggestion that GPSRO refractivity profiles derived with the Abel transform should be interpreted as "mesoscale-sized along-track averages" (Melbourne *et al.* 1994). The operator is composed of two steps. Firstly, a profile of phase-delays is calculated assuming a straight line path through the occultation plane. These delays are then inverted with an Abel transform. This forward-inverse calculation provides a 2D kernel that is used to weight the refractivity values derived from the NWP model. Simulations through an idealised frontal region have suggested an order of magnitude reduction in the errors in the derived refractivity in some cases. However, as yet there are no results demonstrating that this non-local operator produces a statistically significant improvement in the fit to observations when compared with a 1D refractivity operator. It is also unclear why this method is not sensistive to errors in the tangent height, resulting from the use of the derived impact parameter, a; there is no obvious reason why this error should be corrected or reduced as part of the forward-inverse procedure. Sokolovskiy *et al.* (2005) proposed assimilating the intermediate phase-delay directly, but it can be shown that this is equivalent to using the non-local refractivity operator, although Sokolovskiy *et al.* suggest that the assimilation of the phase may be a more computationally efficient approach. Neither of these methods is expected to be more accurate than the assimilation of bending angles with a reasonable 2D operator. In fact, both the non-local refractivity and phase approaches require additional preprocessing of the observations to refractivity, and this complicates the observation errors and will introduce additional correlations. Nevertheless, there are thought to be two main advantages as a result of assimilating GPSRO measurements with these operators, rather than a 2D bending angle operator; the non-local refractivity/phase operators do not require extrapolation of the NWP information above the model top and they are not computationally expensive. In practice, these issues do not represent a major obstacle to the use of 2D bending angle operators. For example, the bending above the ECMWF NWP model top – which increased in height from $\sim$ 65 km to $\sim$ 80 km in February 2006 – can be estimated with sufficient accuracy with an analytical expression, and it is not a significant source of forward model error (HT06). Furthermore, the computational cost of the 2D bending angle operators presented in section 3 is insignificant in the context of the data assimilation process as a whole.

[1] It is not obvious whether the ray tangent height error should be called an observation or forward model error, but we use the combined observation and forward model errors to weight the observations in the assimilation so the distinction is academic.

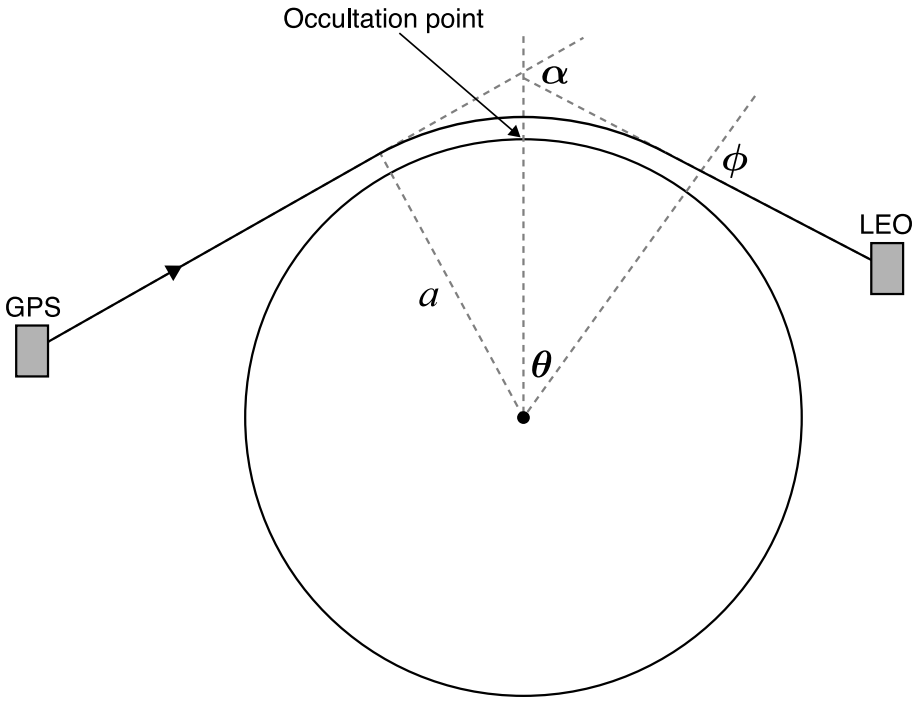

Figure 1: The geometry of the GPSRO measurement technique.

3 Two-dimensional bending angle operators

3.1 Approach 1

The first approach is based on earlier work by Eyre (1994), but it can also be viewed as a generalisation of the 1D operator described in HT06. The main difference between the 2D and 1D operators is that the former evaluates the ray bending using the vertical refractivity gradient at the horizontal position within the 2D plane, θ, whereas the latter always uses the refractivity gradients at the "occultation point" (See Kuo *et al.* 2004).

The geometry of the observation is illustrated in Fig. 1. The two-dimensional plane is defined by the latitude and longitude of the occultation point and an azimuthal angle relative to north, provided with the observation. The NWP profile information is extracted at 31 equally spaced locations in the occultation plane, centred on the occultation point. The angular spacing between the profiles is $\Delta\theta_p = 6.27844 \times 10^{-3}$ radians, corresponding to a horizontal separation at the Earth's surface of $\sim$ 40 km, so the total width of the planar section is $\sim$1200 km (=30$\times$ 40 km). The refractivity, N, and radius, r, are evaluated on the full model levels (see HT06) at each horizontal location. The refractivity, N, is then interpolated onto a fixed vertical grid with 250 points and a 250 m separation, assuming ln$N$ varies linearly with radius. The refractive index-radius product values, $x = r(1+10^{-6}N)$, are evaluated on the 250 m grid.

It is important clearly to outline any major simplifications or approximations that are made in the observation operator. We assume that the occultation point, which corresponds to a ray tangent height of 3 – 4 km above the surface (Kuo *et al.* 2004), defines the horizontal location of the tangent point for each ray in the observation profile, meaning that tangent point drift is neglected. A recent study (von Engeln 2006) has shown that the horizontal location of ray tangent points between surface and a height of 10 km difts by $\sim$ 80 km in the mid-latitudes. This suggests that the error in the tangent location in the lower-troposphere is of order 40 km. The

second major assumption is that the tangent height, r_t, is derived from the impact parameter, a, using $r_t = a/n_t$, where n_t is the refractive index at the tangent point. Note that this assumption is also used in the operator suggested by Poli (2004) and it appears to be implicit in the methods proposed by Syndergaard *et al.* (2005) and Sokolovskiy *et al.* (2005).

The bending angle calculation proceeds as follows. Assume that a point on the ray-path has an angular co-ordinate, θ, and is at the ith vertical level. N and x on the ith and $(i+1)th$ levels are interpolated to θ and the bending associated with the section of path between the ith and $(i+1)th$ levels is given by integrating

$$\Delta\alpha(a) = -a\int_{x_i}^{x_{i+1}} \frac{\frac{d\ln n}{dx}}{(x^2-a^2)^{1/2}}dx \tag{2}$$

After making some simplifications, this integral can be solved in terms of the Gaussian error function (see section 2, HT06). The change in angular position can be written as

$$\Delta\theta = \Delta\alpha - \Delta\phi \tag{3}$$

where $\Delta\phi$ is the change angle between the ray vector and the local radius vector. It can be approximated with

$$\Delta\phi \simeq \sin^{-1}(a/x_{i+1}) - \sin^{-1}(a/x_i) \tag{4}$$

The impact parameter is then updated using the model estimate of the horizontal refractive index gradient

$$\Delta a = \left(\frac{\partial n}{\partial\theta}\right)_r \Delta s \simeq \left(\frac{\partial n}{\partial\theta}\right)_r \times \left(\frac{r_i + r_{i+1}}{\sin\phi_i + \sin\phi_{i+1}}\right) \times \Delta\theta \tag{5}$$

This is repeated until the ray reaches the top of the 250 m vertical grid at 62.25 km. The bending above the model top can be approximated to sufficient accuracy with an analytical expression, based on the complementary error function (Eq.8, HT06). The total bending is given by adding the bending along the section of path between the tangent point and the LEO to the bending along the path between the tangent point and GPS satellite.

The computational time required for the bending angle routine to simulate a typical profile containing 160 bending angles on a 2.4 GHz Pentium 4 pc has been estimated with the F90 "cpu time" command, and it is $\sim$ 0.08 s. This should be compared with a timing of 0.0014 s using the 1D operator (HT06). Note also that the cpu time required to simulate 500 IASI radiances on a 2.4 GHz Pentium 4 pc is $\sim$ 0.08 s (M. Matricardi, pers. comm. 2006).

3.2 Approach 2

Approach 2 is based on solving the differential equations defining the ray-path. It uses the same horizontal grid as in approach 1. Again, the refractivity, N, and radius, r, are evaluated on the full model levels, but it is not necessary to interpolate on to the 250 m vertical grid because the step-length is adjusted as part of the model. As in approach 1, tangent point drift is neglected and the derived impact parameter is used to determine the tangent point height.

The bending angle calculation is based on a numerical solution of the differential equations defining the ray-path in circular polar co-ordinates (r and θ) (e.g., page 149, Rodgers, 2000)

$$\frac{dr}{ds} = \cos\phi \tag{6}$$

$$\frac{d\theta}{ds} = \frac{\sin\phi}{r} \tag{7}$$

$$\frac{d\phi}{ds} = -\sin\phi\left[\frac{1}{r} + \frac{1}{n}\left(\frac{\partial n}{\partial r}\right)_\theta\right] + \frac{\cos\phi}{nr}\left(\frac{\partial n}{\partial \theta}\right)_r \tag{8}$$

where s is the distance along the ray-path, n is the refractive index, ϕ is angle between the local radius vector and the tangent to the ray-path. In practice, Eq.8 can be simplified by assuming $1/n \sim 1$ and noting that near the tangent point, where the ray bending is largest, $\phi \simeq \pi/2$, so $\cos\phi \times (\partial n/\partial\theta)_r \simeq 0$. Physically, this term is small because the ray-path is almost parallel with $(\partial n/\partial\theta)_r$ near the tangent point. Ray bending is caused by the component of the refractivity gradient that is perpendicular to the path. Hence, eq.8 simplifies to

$$\frac{d\phi}{ds} \simeq -\sin\phi\left[\frac{1}{r} + \left(\frac{\partial n}{\partial r}\right)_\theta\right] \tag{9}$$

Simulations indicate that the bending angle errors caused by these approximations are less than 0.05%. The equations are solved with the 4th order Runge-Kutta method. The step-length is adjusted along the ray-path. Consider the section of ray-path between ith and (i+1)th model levels. The path is split into m steps (currently m=10). We define a radial increment given by $\Delta r = (r_{i+1} - r_i)/m$, where r_i and r_{i+1} are the radius values on the ith and $(i+1)th$ model levels, and choose the step-length, Δs, so that the change in r is approximately Δr. At the tangent point the step-length is given by $\Delta s = \sqrt{2 r_t \Delta r}$, where r_t is the radius value of the tangent point. More generally, the step-length is given by $\Delta s = \Delta r/\cos\phi$. The radial refractivity gradient is calculated assuming that refractivity between the model levels varies exponentially with height. Bending above the model top uses the analytical method noted in approach 1.

The above represents a ray tracing observation operator. Ray tracers have been described as "*theoretically* the best observation operators" (Poli 2004), but have been considered impractical for operational NWP centres because of the computational expense. However, the computational cost is not prohibitive; one profile containing 160 bending angles can be simulated in ~ 0.25 s on the 2.4 GHz Pentium 4 pc.

4 4D-Var assimilation experiments

The 4D-Var assimilation (Rabier *et al.* 2000; Klinker *et al.* 2000) experiments use cycle 29R1 of the ECMWF system and are run in the early-delivery mode (Haseler, 2004). The forecast model has 60 levels in the vertical, the horizontal resolution is T511 and the 4D-Var increments are at T159. The GPSRO measurements have been processed by UCAR (Kuo *et al.* 2004), but have been interpolated and thinned onto 180 fixed impact heights between the surface and 40 km (HT06). The impact height, h, is defined as $h = a - R_c$, where R_c is the radius of curvature for the observation. The standard deviations of the combined observation/forward model errors are assumed to vary with h. The percentage error is assumed to be 10% of the observed value at $h = 0$, falling linearly with h to 1% at $h = 10$ km. Above 10 km, the error is assumed to be 1% of the observed value until this reaches a lower limit of 6×10^{-6}radians. The errors are assumed to be uncorrelated. Note that the same error model is used in both the 1D and 2D experiments, which may appear questionable in the lower-troposphere given that the 2D operators are expected to be more accurate. As noted in section 2, the errors used here are somewhat larger than those presented in Poli and Joiner (2004), but Poli and Joiner do not include the errors associated with using an incorrect tangent height, so the values used in this study probably represent a more accurate estimate of the combined observation/forward errors required for assimilation. Furthermore, a 4D-Var diagnostic which is based on the GPSRO contribution to the observation cost function value at the analysis state, normalised by the number of bending angles that have been assimilated, indicates that the error model is reasonable for both the 1D and 2D operators.

In contrast to HT06, all the bending angles with impact heights below 5 km that pass the first-guess departure (Järvinen and Undén, 1997) and the variational (Andersson and Järvinen, 1999) quality control steps have been assimilated, in order to investigate the impact of the 2D operators in the lower-troposphere. In addition, the GPSRO surface pressure increments are included in this study. These arise because the integration of the hydrostatic relationship is part of the bending angle observation operators.

4.1 Single profile experiments

In the single profile experiments all measurements are blacklisted except one CHAMP GPSRO bending angle profile. The aim is to demonstrate how the use of 2D operators modifies the analysis increments. In this example the CHAMP profile is measured on the 1st June 2004 at 00 UTC, which is 3 hours after the start of the assimilation window. It is located at (19.8N,71.6E) and the occultation plane is at an angle of 19° relative to north. This profile was chosen because it contains bending angles that reach to within 3 km of the surface in a region with relatively large specific humidity values.

Intuitively, we might expect the increments to be significantly broadened with the use of the 2D operators, but it is important to recognise that the background error covariance matrix, **B**, plays a fundamental role in spreading information in the horizontal. Figure 2 shows the analysis minus forecast temperature increments on model level 29 ($\sim$ 177 hPa), evaluated with the 1D operator (a), the 2D operator described in section 3.1 (b) and the 2D operator described in section 3.2 (c). Although the 2D operators produce slightly broader increments, they do not change the shape or magnitude of the increments significantly. In fact, Figure 2a clearly illustrates how the 4D-Var background error covariance matrix smooths the temperature increments in the horizontal, even though the observation is assumed to be a profile measurement. This is because the 4D-Var assimilation system expects the forecast errors to be large-scale and smooth. This enables the analysis increments to be calculated on a T159 grid, corresponding to $\sim$ 125 km in the horizontal. It is interesting to compare the spatial extent of the increments with the width of the bending angle weighting function along a ray-path. To first order (Melbourne *et al.* 1994), assuming that the refractivity falls exponentially with height, the horizontal weighting function, $d\alpha/ds$, has a Gaussian shape given by,

$$\frac{d\alpha}{ds} \propto \exp\left(-\frac{s^2}{2Hr_t}\right) \tag{10}$$

where s is the distance from the tangent point, H is the refractivity scale-height and r_t is the radius of the tangent point. Assuming $H \sim 6$ km and $r_t \sim 6371$ km, approximately 68% of the bending takes place over a 400 km section of path, centred on the tangent point. Therefore, a typical bending angle horizontal weighting function is quite small, when compared with the spatial scale of the temperature increments in the horizontal.

It could be argued that the 2D operators are not expected to change the temperature increments in the upper-troposphere and lower-stratosphere, and the largest differences should be expected in the lower-troposphere. Figure 3 shows the specific humidity (Q) increments on model level 47, at a pressure of $\sim$ 797 hPa. Note that the spatial scale of the Q increments are considerably smaller than the temperature increments, and there is some indication that they are being broadened with the 2D operators.

4.2 Forecast impact experiments

Forecast impact experiments have been conducted with CHAMP measurements for the period 1st June, 2004 to 31st July, 2004. Four experiments have been performed:

1) The "control" experiment (CTL) assimilates the set of conventional and satellite measurements that are used operationally.

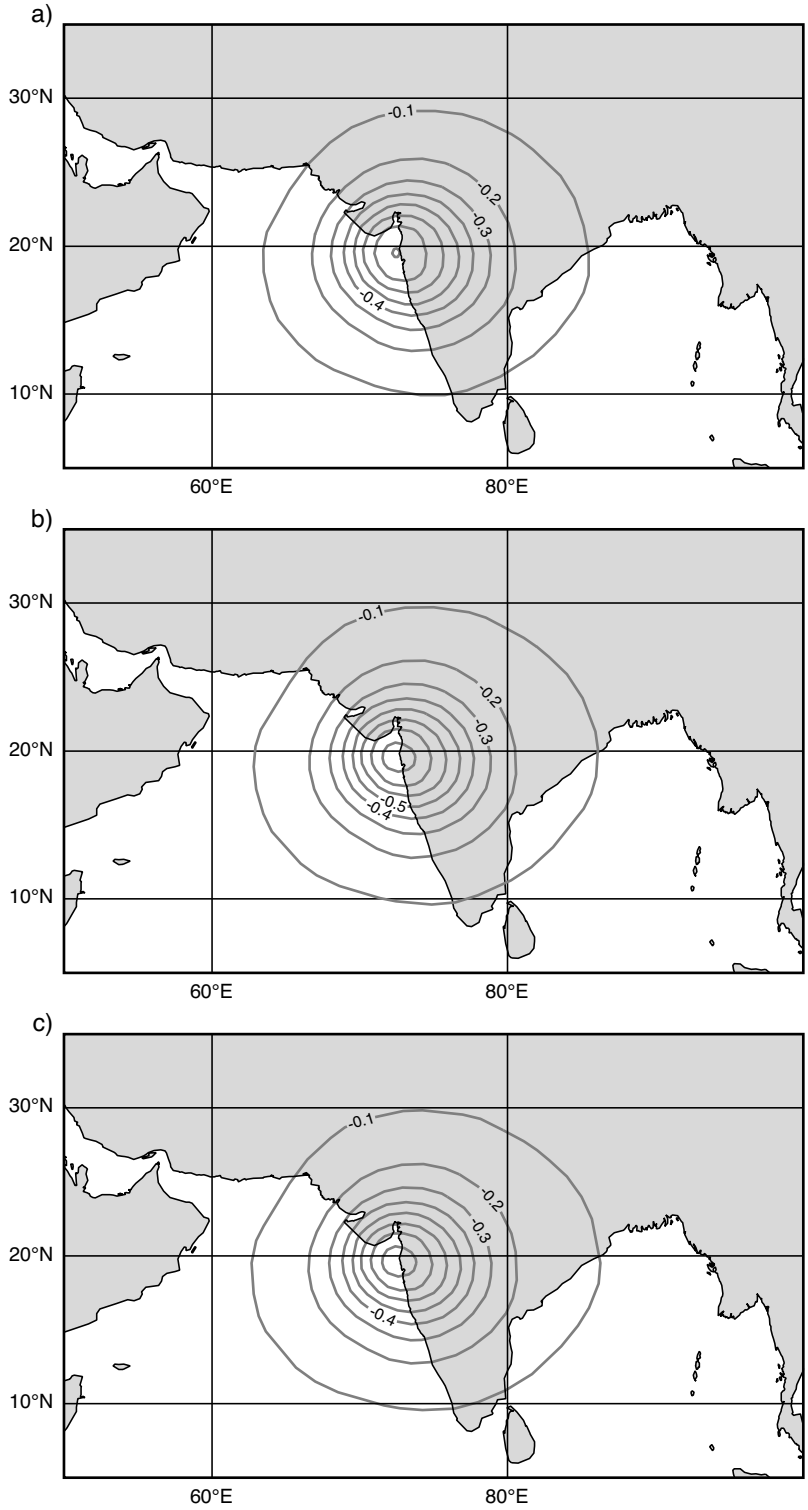

Figure 2: The temperature increments at model level 29 with the 1D operator (a), the 2D operator described in section 3.1 (b) and the 2D operator described in section 3.2 (c). The contour lines have a 0.1K interval.

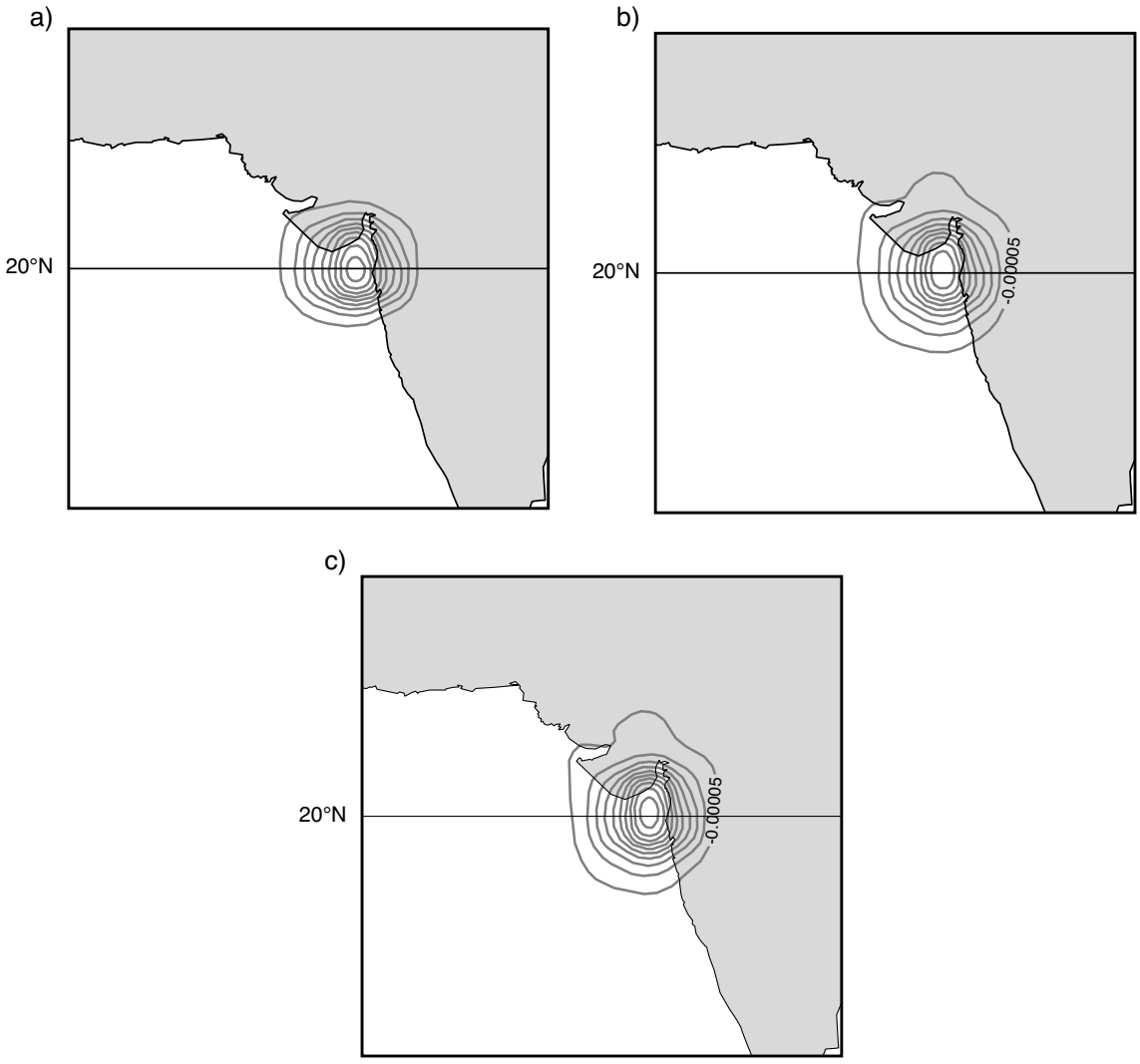

Figure 3: The specific humidity increments at model level 47 with the 1D operator (a), the 2D operator described in section 3.1 (b) and the 2D operator described in section 3.2 (c). The contour lines have a 5×10^{-5} *Kg/Kg interval.*

2) The "1D" experiment is identical to the CTL, except that GPSRO bending angles are assimilated with the 1D bending angle operator described in HT06.

3) The "2D" experiment is identical to the CTL, except that GPSRO bending angles are assimilated with the 2D operator described in section 3.1.

4) The "2DRK" experiment is identical to the CTL, except that GPSRO bending angles are assimilated with the 2D Runge-Kutta solution of the ray equations described in section 3.2.

The statistics of the observed minus background (O-B) and observed minus analysis (O-A) departure distributions are a useful diagnostic. The O-B departures should represent the diagonals of the $\mathbf{HBH^T} + \mathbf{E} + \mathbf{F}$ matrix, where $\mathbf{H}$ is the linearised observation operator and $\mathbf{B}$, $\mathbf{E}$ and $\mathbf{F}$ are the background, observation and forward model error covariance matrices, respectively. Ideally, the use of the 2D operators should reduce the forward model error component. We have found that the 2D observation operators reduce the width of the observed minus background (O-B) and observed minus analysis (O-A) bending angle departure distributions in the northern and southern hemispheres. As expected, the largest improvements with the 2D operators are in the lower-troposphere. A typical example is Figure 4, which shows the O-B and O-A bending departures in the southern hemisphere for the the 1D (grey) and 2D (black) experiments, for impact heights, h, between $\sim$ 4.5 km and 6 km. More generally, in the northern and southern hemispheres the root-mean-square (RMS) of the O-B departure distributions with the 2D operators are $\sim$ 5% smaller than for 1D operator, for $h < 6$ km. The improvements in the O-B are smaller when $h > 6$km and they are generally less than 1% for $h > 10$ km. There are no significant differences in the O-B distributions in the 2D and 2DRK experiments, indicating that the forward operators described in sections 3.1 and 3.2 are of comparable accuracy.

There is no clear improvement O-B bending angle departures in the tropics as a result of using the 2D operators, and in fact the departures with $h < 6$ km are biased low (Rocken *et al.* 1997; Ao *et al.* 2003) for all three GPSRO experiments. However, note that the first-guess departure quality control procedure (Järvinen and Undén, 1997) rejects around 2 – 3% of the measured bending angles and this reduces the bias by around 20%. For example, in the 2D experiment 3125 observed bending angles with impact heights, h, between 3.3 km and 4.3 km, are processed in the tropics and the mean O-B departure is -1.36×10^{-3} radians, but the first-guess departure check removes 83 bending angles and this reduces the bias to -1.09×10^{-3} radians.

GPSRO measurements provide useful temperature information in the upper-troposphere and lower-stratosphere, particularly in the southern hemisphere. Figure 5 shows the forecast and analysis fit to radiosonde temperature measurements over Antarctica. It is noticable that all three GPSRO forward models improve both the mean and standard deviation of the fit to the radiosondes. However, there does not appear to be any significant additional improvement as a result of using 2D observation operators. Note that the sharp structure in the mean fit of the CTL experiment is an example of the ECMWF's "stratospheric ringing" problem (A.P. McNally, pers. comm. 2005). This arises because the radiance measurements introduce large temperature increments at the upper model level at the winter pole. The vertical correlation structure in the background error covariance matrix then spreads this information down the profile, superimposing an oscillatory perturbation on the stratospheric temperatures. The ringing is illustrated in Figure 6, which shows the mean temperature analysis on the model levels over Antarctica (south of 60S) for the CTL and 2D experiments, averaged over the two month period (Virtually identical results are obtained with 1D and 2DRK experiments.). It is clear that the GPSRO observations produce a considerably smoother mean analysis state over Antarctica which is more consistent with the radiosonde measurements (Figure 5). The GPSRO measurements are unable to smooth out the kink near model level 8 (2.7 hPa) because the information content of the bending angles falls rapidly with height, and only bending angles with impact heights less than 40 km are assimilated.

The forecast fit to radiosonde measurements in the southern hemisphere between 300 hPa - 50 hPa, over the day-1 to day-5 range, is shown in Figure 7. It is clear that assimilating GPSRO measurements improve the analyses

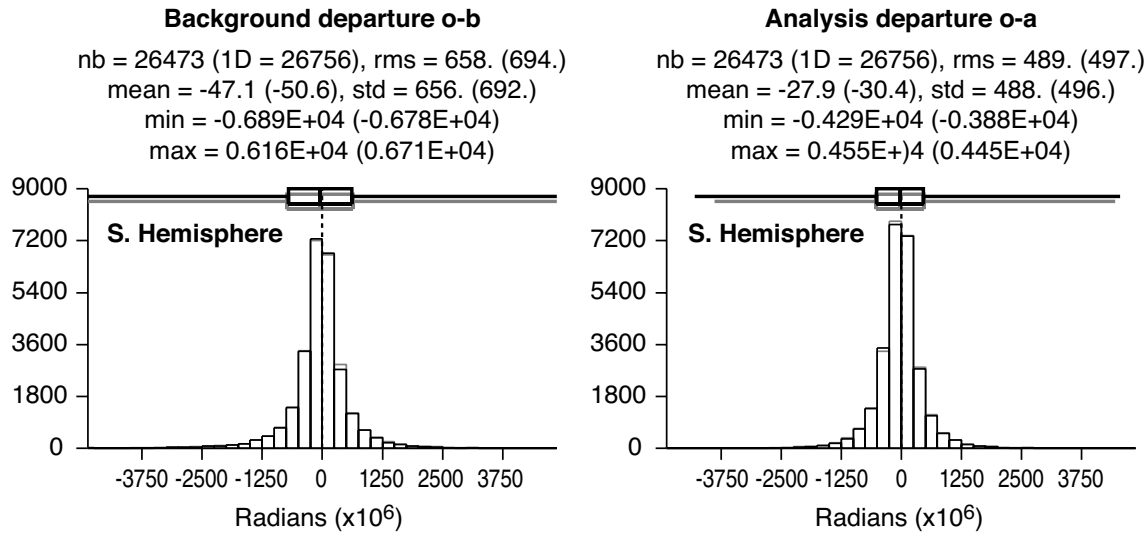

Figure 4: The O-B and O-A bending angle departures for the 2D (black) and 1D (grey) experiments in the southern hemisphere, for impact heights between 4.5 km and 6 km. The statistics for the 1D departures are within the brackets.

and the subsequent forecasts. For example, the improvements at 50 hPa are statistically significant at the 0.1% level. It should be emphasised that this is an extremely encouraging result. However, the scores with the 1D and 2D operators are very similar. More generally, the temperature scores against radiosondes in the northern hemisphere are neutral for each of the GPSRO experiments. In the tropics, the GPSRO measurements reduce a known cold model bias of $\sim$ -1 K at 100 hPa by $\sim$ 0.05K, but they also increase a cold model bias at 50 hPa from from $\sim$ -0.35 K to -0.5 K. This appears to be related to oscillations in the mean fit to radiosondes, similar to those shown in Figure 5, but with a smaller amplitude of $\sim$ 0.5 K. The GPSRO measurements tend to smooth the mean departure profile, reducing the mean differences and increasing the data usage at 100, 70, 30 and 20 hPa, but degrading the fit at 50 hPa. Again there are no clear differences between assimilating the GPSRO measurements with the 1D and 2D models, and overall the results suggest that assimilation with 2D operators does not significantly improve the temperature information that can be derived in the upper-troposphere and lower-stratosphere. This is not entirely surprising because the 2D operators are expected to have the largest impact in the lower-troposphere, where the horizontal gradients in refractivity are largest.

In the lower-troposphere HT06 adopted a conservative approach by blacklisting all bending angles with impact heights below 5 km. Despite this it was found that the GPSRO measurements were introducing large surface pressure increments over Antarctica, which were degrading the 500 hPa geopotential height (500Z) field. Consequently, it was necessary to introduce an ad-hoc modification of the tangent-linear and adjoint of the GPSRO forward model to remove the sensitivity of the model level heights to surface pressure. However, in this study all the bending angles down to the surface that pass the first-guess and variational QC criteria are assimilated, and the sensitivity to surface pressure has been re-introduced, without degrading the surface pressure and 500Z analyses. Figure 8 shows the RMS of the 1D-CTL surface pressure analysis differences, averaged over the 2 month period. The largest differences are $\sim$ 0.25 hPa. In the previous forecast impact experiments (Figure 2, HT06) the RMS differences exceeded 2.5 hPa. This improvement is not a result of changes to the 1D operator or better quality GPSRO observations. In fact, it appears to be a result of recent developments in the processing in surface pressure observations at ECMWF that have been implemented in cycle 29R1. (Drasko Vasiljevic, pers. comm. 2005). ECMWF have introduced a bias correction scheme for surface observations and re-tuned the observation error estimates to increase the weight given to automatic synop and drifting buoy measurements. Automatic synop errors have been reduced from 0.7 hPa to 0.52 hPa and drifting buoy errors

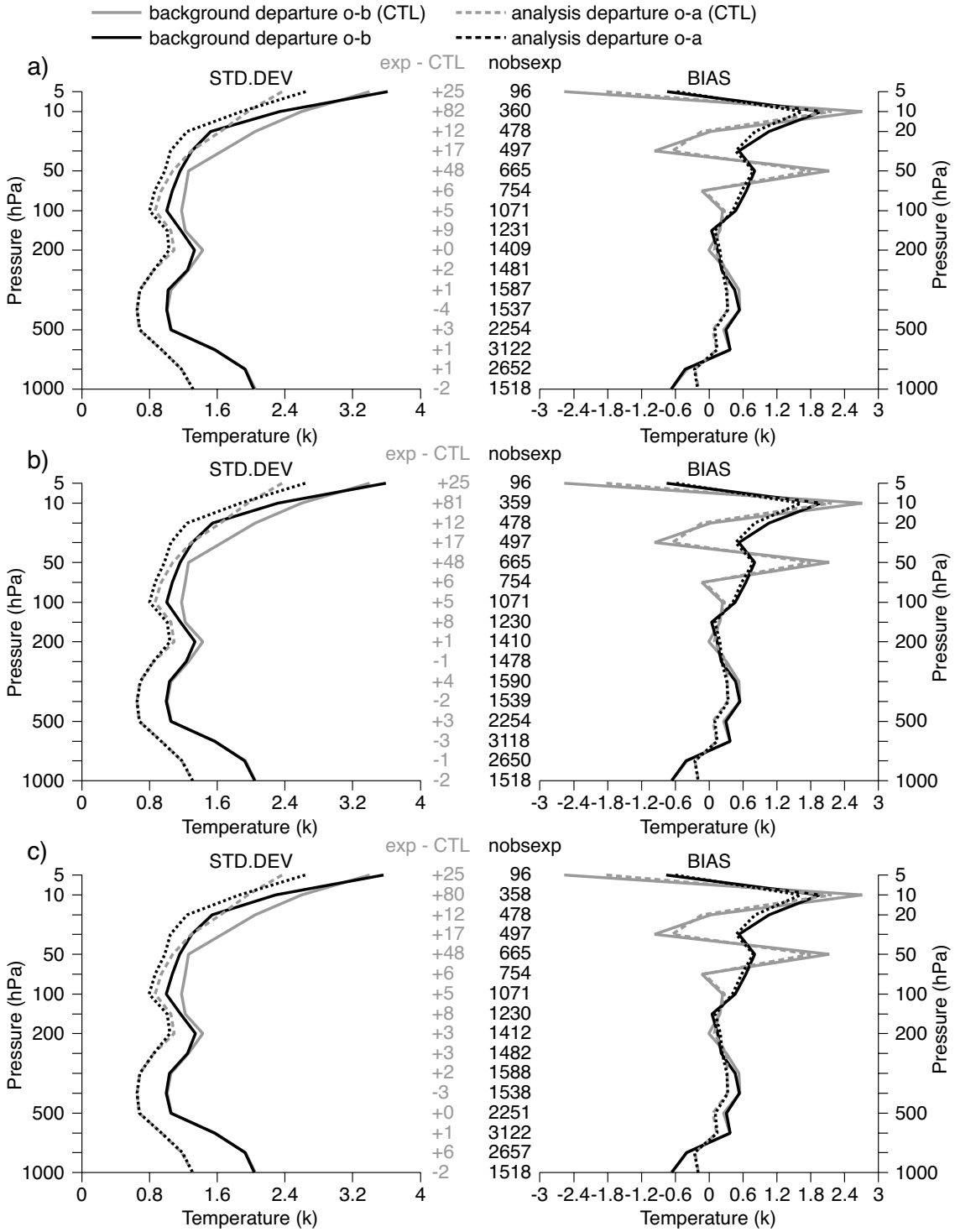

Figure 5: The standard deviation and bias of the 12h forecast and analysis fit to radiosondes (radiosonde - NWP) in Antarctica for the 1D (top), 2D (middle) and 2DRK (bottom) experiments (all black) compared with the CTL (grey) experiment. The central column gives the number of comparisons on the pressure levels.

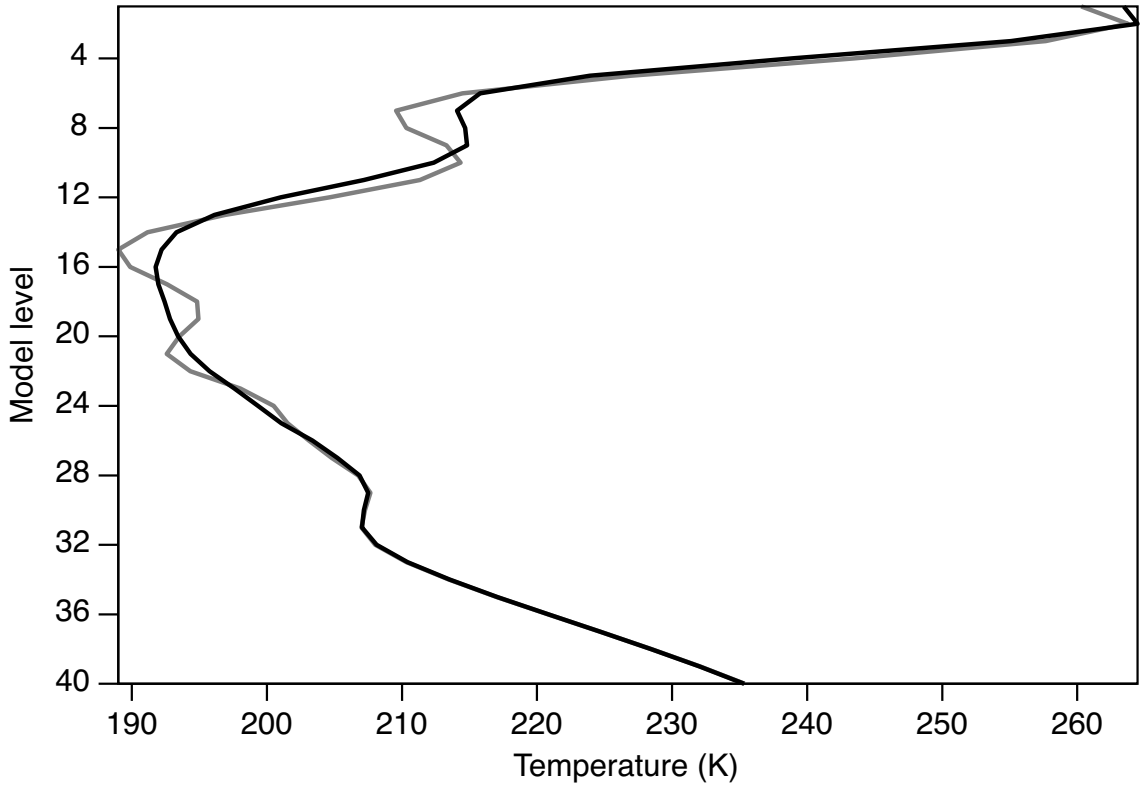

Figure 6: The mean temperature analyses over Antarctica on model levels for the CTL (grey) and 2D (black) experiments, averaged from 1st June – 31st July, 2004.

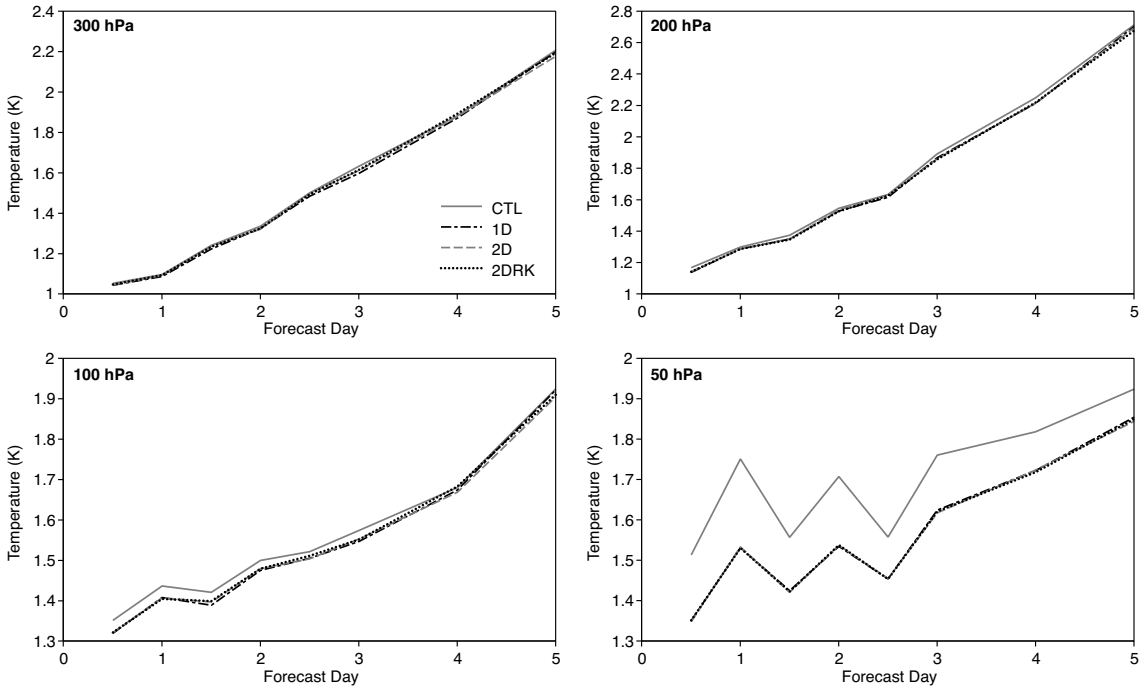

Figure 7: The RMS fit to radiosonde temperatures at 300, 200, 100 and 50 hPa in the southern hemisphere for the CTL, 1D, 2D and 2DRK experiments.

have been reduced from 0.88 hPa to 0.62 hPa. The analysis fit in the southern hemisphere to both drifting buoys and synops has subsequently improved to less than 0.5 hPa and it appears that the surface pressure analysis in the southern hemisphere is now far more constrained. This effectively reduces the weight given to the GPSRO surface pressure information during the assimilation.

Figure 9 illustrates the 500Z anomaly correlation (AC) for the CTL and GPSRO experiments in the southern hemisphere, averaged over 51 cases. In contrast to the original experiments presented in HT06, it is now difficult to distinguish between the CTL and the three GPSRO experiments when the surface pressure increments are included. In fact, statistical significance testing indicate that the GPSRO observations produce a small improvement in the AC at the day-1 and day-2 forecast-range, then degrade the score slightly around the day-6 and day-7 range. This is illustrated in Figure 10, where the error bars show the 5% significance level. Similar results are found for 500Z RMS error when verified against analyses and observations. The differences between between the 500Z scores using the 1D and 2D GPSRO operators over the day-1 to day-8 forecast range are not statistically significant for this 2 month period. Nevertheless, it is encouraging that these results are obtained assimilating GPSRO observations without introducing ad-hoc modifications to the observation operators or bias correction procedures.

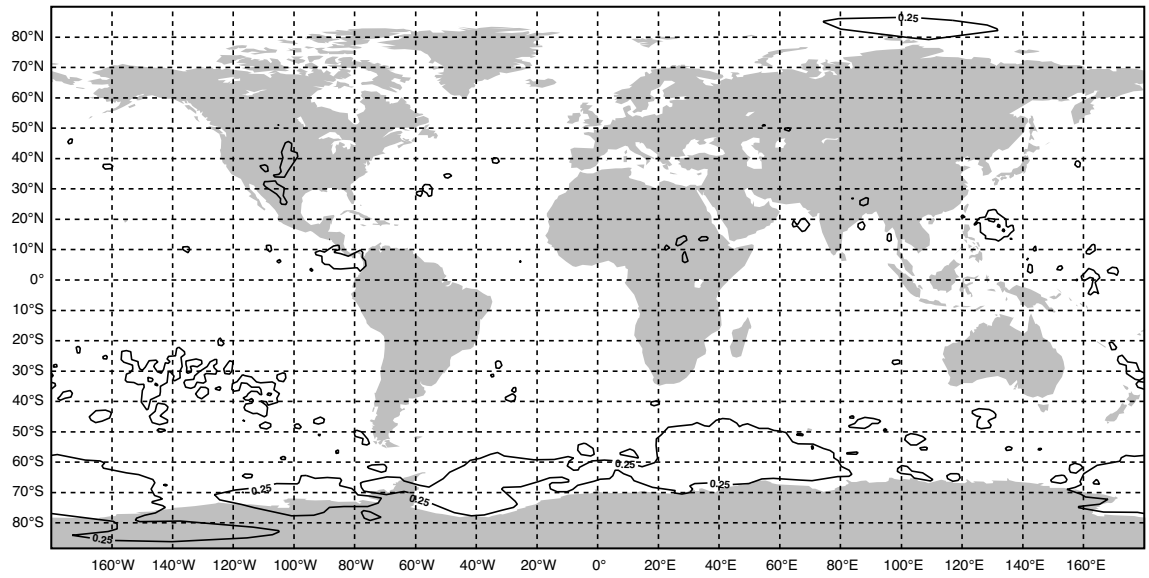

Figure 8: The RMS differences of the 1D - CTL surface pressure analyses, averaged from 1st June to 31st July, 2004 . The contour lines have a 0.25 hPa interval.

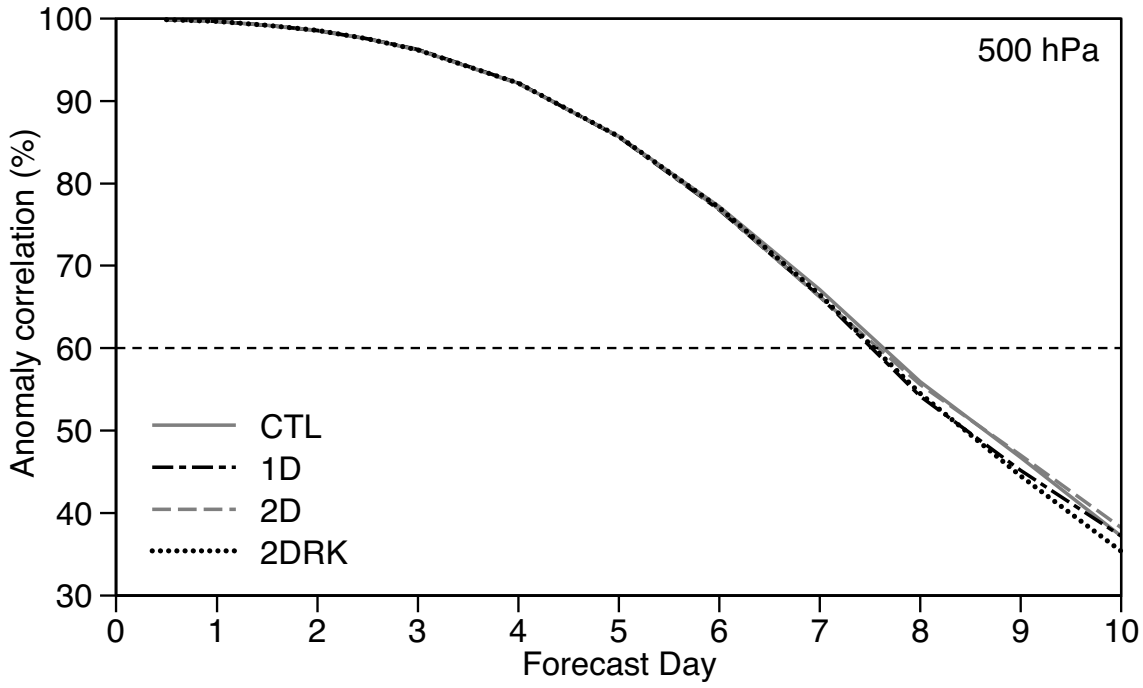

Figure 9: The anomaly correlation at the 500Z level in the southern hemisphere for the CTL, 1D, 2D and 2DRK experiments, averaged over 51 days between 1st June and 21st July, 2004.

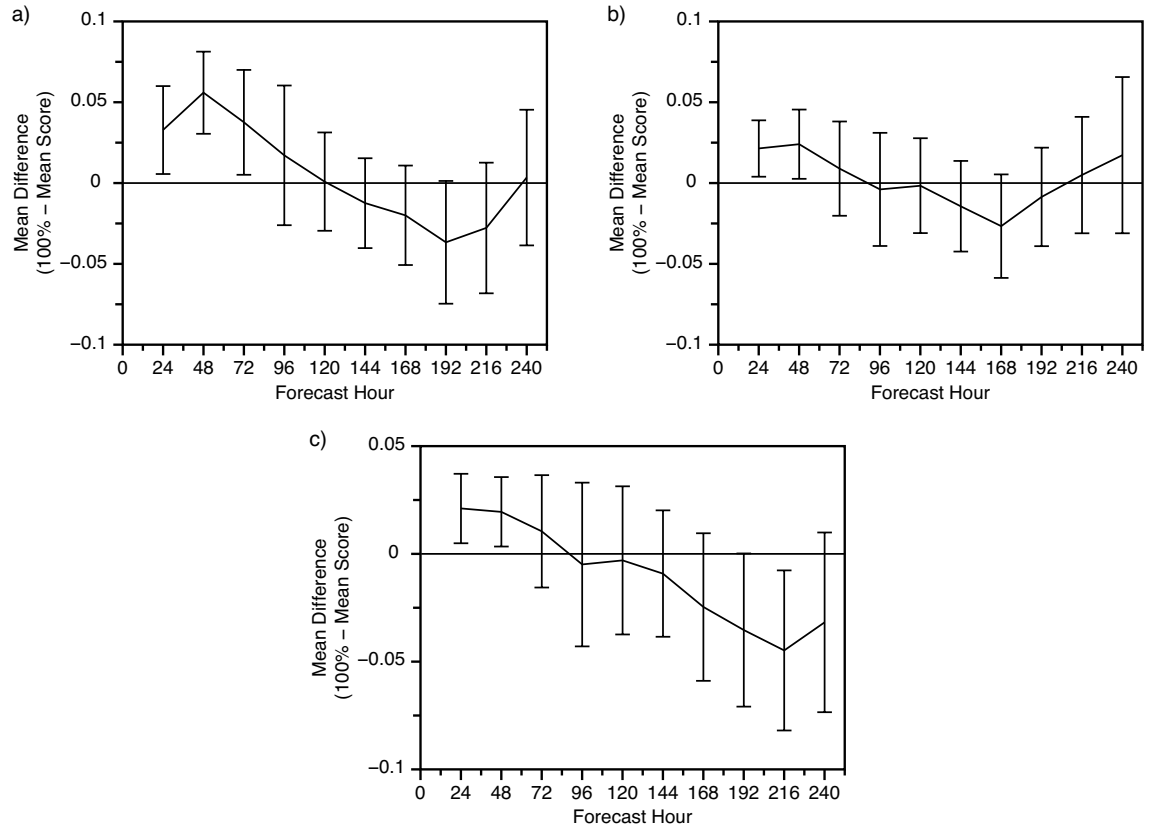

Figure 10: The statistical significance of the 500Z AC differences in the southern hemisphere as a function of forecast hour for (a) 1D, (b) 2D and (c) 2DRK experiments versus the CTL.

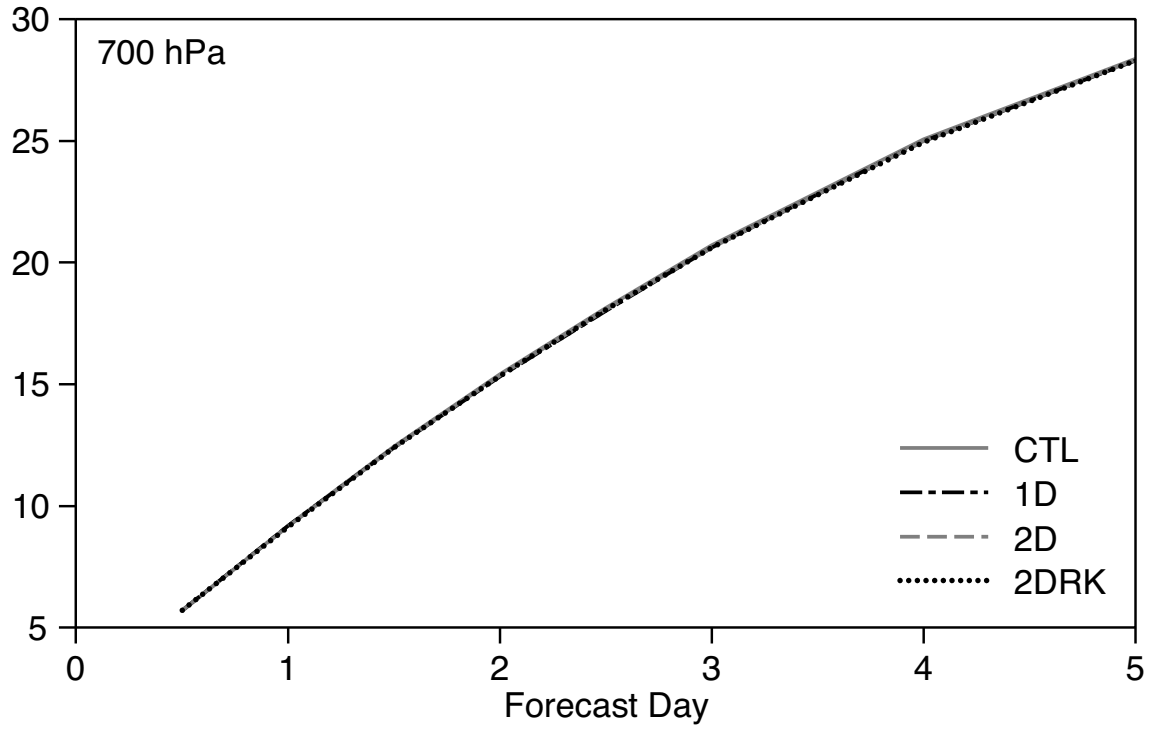

Figure 11: The relative humidity forecast errors (%) at 700 hPa in the southern hemisphere for the CTL, 1D, 2D and 2DRK experiments, each verified against their own analyses.

We have investigated the relative humidity forecast scores at 1000, 850, 700 and 500 hPa for the four experiments, with each experiment verified against its own analysis. There is no clear reduction in the size of the humidity analysis increments and in general the differences in the forecast scores over the day-1 to day-5 forecast range are small as, for example, illustrated in Figure 11, which shows the forecast scores at 700 hPa in the southern hemisphere. Although some of the forecast scores appear to have statistically significant differences, the size of the differences mean that they are unlikely to be physically meaningful. However, one interesting aspect of the results is that the bending angles in the tropical lower-troposphere – which are biased low compared with those simulated with the NWP foercast state – do not appear to be producing a dry bias in the model state.

5 Discussion and Conclusions

The results illustrate that using 2D bending angle operators rather than a 1D approach reduces the RMS of the O-B distributions by around 5%, for impact heights $h < 6$ km in the northern and southern hemispheres. The reduction in the width of the O-B distributions falls with impact height, and is generally less than 1% for $h > 10$ km. However, the improvement in the O-B departures does not appear to produce significantly better forecast scores in the lower-troposphere, which are generally neutral in all three GPSRO experiments. This may be a consequence of the limited accuracy of the observations in the lower-troposphere as a result of the current processing methods. However, it also possibly indicates that a single instrument, CHAMP, simply does not provide enough observations to sample, on a regular basis, those cases where the improved forward modelling could produce a significant positive forecast impact. These issues will be investigated further when open-loop processing is implemented and more measurements from GRAS and COSMIC are available. Nevertheless, we believe that a neutral impact represents a reasonable step forward because it has been achieved without blacklisting bending angles near the surface or introducing the ad-hoc modifications to the 1D observation operator required in HT06. The observed bending angles in the tropical lower-troposphere appear to be biased low, but the size of the bias is reduced by $\sim 20\%$ as a result of the first-guess departure QC check (Järvinen and Undén, 1997). The remaining bias does not appear to introduce a bias in the tropical humidity fields, but again this may be a consequence of the low number of measurements. It should be emphasised that the assimilation of the GPSRO measurements results in a clear improvement in the RMS fit to lower-stratospheric radiosonde temperature measurements in the southern hemisphere using both the 1D and 2D operators, but there is no clear additional improvement associated with using the 2D operators for this two month period. This suggests that the 1D operators are sufficiently accurate in this region.

We have investigated two 2D bending angle observation operators and have found that they both provide a similar reduction in the RMS of the O-B distributions, when compared with the 1D results. It must be emphasised that the computational cost of the 2D operators is not prohibitive and it has been demonstrated that they can be implemented within an operational NWP system. Although the Runge-Kutta solution of the ray-path equations (section 3.2) may be theoretically more appealing, we have found that the models provide bending angles of similar accuracy. In both cases, the accuracy of the simulated bending angles is probably determined more by how the problem has been approximated, rather than the subsequent numerical solution of the approximated problem. The most significant approximations made in both 2D operators are the neglect of tangent point drift and the use of the derived impact parameter to determine the tangent height of the ray. Poli and Joiner (2004) have shown that including tangent point drift can reduce the standard deviation of the O-B bending angle distribution by $\sim 10\%$ in the northern and southern hemispheres for tangent heights around 18 km, but reduction is only of order 1% in the lower-troposphere. We believe that the fixed tangent point assumption used in this study is acceptable because the occultation point corresponds to a ray tangent height of 3 – 4 km (Kou *et al.* 2004) and, as noted in section 3.1, it should only introduce horizontal location errors of order 40 km in the lower-troposphere, for measurements in the mid-latitudes (von Engeln 2006). Although it may be desirable to reduce the errors around 18 km, it is clearly not essential as the forecast impact experiments with 1D operators have demonstrated (Healy *et al.* 2005; HT06). Furthermore, we have performed simulations in the domain of a 12 km by 12 km mesoscale model indicating that in the lower troposphere the errors caused by the incorrect tangent height are larger than the tangent point drift errors (unpublished). It is possible to attempt to correct the tangent height error using the horizontal gradient estimates derived from the NWP forecast model. One approach is based on calculating the impact parameter value at the GPS and LEO satellites, denoted by a_g and and a_l respectively, as part of the 2D operator. These values are then used to estimate the impact parameter value that would be derived from the Doppler shift, a_d, with

$$a_d = \gamma a_l + (1-\gamma) a_g \tag{11}$$

where γ is a scalar that depends on the geometry of the occultation and the velocity of the satellites (See Eq. A5 and A11, Healy, 2001). The forward modelled profile, $\alpha(a_d)$, can then be interpolated to the "observed" impact parameter values. The potential benefits of this approach will depend on the resolution of the NWP model, as this will determine how accurately the impact parameter variation along the ray-path can be modelled. ECMWF increased the resolution of its operational model to T799 (25 km) in February 2006, so this correction should be investigated as part of ongoing work to improve the 2D bending angle operators.

Acknowledgements

The authors thank Niels Bormann, Sami Saarinen, Lars Isaksen and Christian Marquardt for their help during this study. Stig Syndergaard provided useful comments on an early version of this paper. The authors also acknowledge GFZ-Potsdam and UCAR for providing the CHAMP data and the EUMETSAT GRAS-SAF for providing the 1D bending angle observation operator code. The figures were improved by Anabel Bowen.

Sean Healy is supported through the EUMETSAT/ECMWF Fellowship Programme.

References

Andersson, E., and H. Järvinen, 1999: Variational quality control. *Quart. J. Roy. Meteorol. Soc.*, **125**, 697–722.

Anthes, R., C. Rocken, and Y. Kou, 2000: Applications of COSMIC to meteorology and climatology. *Terrestrial, Atmospheric and Oceanic Sciences*, **11**, 115–156.

Ao, C., T. Meehan, G. Hajj, A. Manucci, and G. Beyerle, 2003: Lower troposphere refractivity bias in GPS occultation retrievals. *J. Geophys. Res.*, **108**, doi:10.1029/2002JD003216.

Cohn, S., 1997: In introduction to estimation theory. *J. Met. Soc. Jap.*, **75**, 257–288.

Collard, A., and S. Healy, 2003: The combined impact of future space-based atmospheric sounding instruments on numerical weather prediction analysis fi elds: A simulation study. *Quart. J. Roy. Meteorol. Soc.*, **129**, 2741–2760.

Eyre, J., 1994: Assimilation of radio occultation measurements into a numerical weather prediction system. Technical Memorandum 199, ECMWF, Reading, UK.

Haseler, J., 2004: Early delivery suite. Technical Memorandum 454, ECMWF, Reading, UK.

Healy, S., 2001: Radio occultation bending angle and impact parameter errors caused by horizontal refractive index gradients in the troposphere: A simulation study. *J. Geophys. Res.*, **106**, 11875–11889.

Healy, S., A. Jupp, and C. Marquardt, 2005: Forecast impact experiment with GPS radio occultation measurements. *Geophys. Res. Lett.*, **32**, LO3804,doi:10.1029/2004GL020806.

Healy, S., and J.-N. Thépaut, 2006: Assimilation experiments with CHAMP GPS radio occultation measurements. *Quart. J. Roy. Meteorol. Soc.*, **132**, 605–623.

Järvinen, H., and P. Undén, 1997: Observation screening and background quality control in the ECMWF 3DVAR data assimilation system. Technical Memorandum 236, ECMWF, Reading, U.K.

Klinker, E., F. Rabier, G. Kelly, and J.-J. Mahfouf, 2000: The ECMWF operational implementation of four dimensional variational assimilation. Part III: Experimental results and diagnostics with operational confi guration. *Quart. J. Roy. Meteorol. Soc.*, **126**, 1191–1218.

Kuo, Y.-H., T.-K. Wee, S. Sokolovskiy, C. Rocken, W. Schreiner, D. Hunt, and R. Anthes, 2004: Inversion and error estimation of GPS radio occultation data. *J. Met. Soc. Jap.*, **82**, 507–531.

Kursinski, E., G. Hajj, W. Bertiger, S. Leroy, T. Meehan, L. Romans, J. Schofi eld, D. McCleese, W. Melbourne, C. Thornton, T. Yunck, J. Eyre, and R. Nagatani, 1996: Initial results of radio occultation observations of earth's atmosphere using the Global Positioning System. *Science*, **271**, 1107–1110.

Kursinski, E., G. Hajj, J. Schofi eld, R. Linfi eld, and K. Hardy, 1997: Observing earth's atmosphere with radio occultation measurements using the Global Positioning System. *J. Geophys. Res.*, **102**, 23.429–23.465.

Liu, H., and X. Zou, 2003: Improvements to a GPS radio occultation ray-tracing model and their impacts on the assimilation of bending angle. *J. Geophys. Res.*, **108**, doi:10.1029/2002JD003160.

Loiselet, M., N. Stricker, Y. Menard, and J.-P. Luntama. Metop's GPS-Based Atmospheric Sounder. ESA Bulletin. No. 102, 2000.

Melbourne, W., E. Davis, C. Duncan, G. Hajj, K. Hardy, E. Kursinski, T. Meehan, and L. Young, 1994: *The application of spaceborne GPS to atmospheric limb sounding and global change monitoring*. Publication 94–18, Jet Propulsion Laboratory, Pasadena, Calif.

Palmer, P., 1998: *Analysis of atmospheric temperature and humidity from radio occultation measurements*. PhD thesis, University of Oxford.

Poli, P., 2004: Effects of horizontal gradients on GPS radio occultation observation operators. 2: A fast atmospheric refractivity gradient operator (FARGO). *Quart. J. Roy. Meteorol. Soc.*, **130**, 2807–2825.

Poli, P., and J. Joiner, 2004: Effects of horizontal gradients on GPS radio occultation observation operators. 1: Ray tracing. *Quart. J. Roy. Meteorol. Soc.*, **130**, 2787–2805.

Rabier, F., H. Järvinen, E. Klinker, J.-J. Mahfouf, and A. Simmons, 2000: The ECMWF operational implementation of four dimensional variational assimilation. Part I: Experimental results with simplified physics. *Quart. J. Roy. Meteorol. Soc.*, **126**, 1143–1170.

Rocken, C., R. Anthes, M. Exner, D. Hunt, S. Sokolovsky, R. Ware, M. Gorbunov, W. Schreiner, D. Feng, B. Herman, Y.-H. Kuo, and X. Zou, 1997: Analysis and validation of GPS/MET data in the neutral atmosphere. *J. Geophys. Res.*, **102**, 29.849–29.866.

Rodgers, C., 2000: *Inverse methods for atmospheric sounding: Theory and practice*. World Scientific Publishing, Singapore, New Jersey, London, Hong Kong.

Sokolovskiy, S., 2001: Tracking tropospheric radio occultation signals from low Earth orbit. *Radio Sci.*, **36**, 483–498.

Sokolovskiy, S., Y.-H. Kuo, and W. Wang, 2005: Assessing the accuracy of a linearized observation operator for assimilation of radio occultation data: Case simulations with a high-resolution weather model. *Mon. Wea. Rev.*, **133**, 2200–2212.

Syndergaard, S., E. Kursinski, B. Herman, E. Lane, and D. Flittner, 2005: A refractive index operator for assimilation of occultation data. *Mon. Wea. Rev.*, **133**, 2650–2668.

von Engeln, A., 2006: An analysis of CHAMP radio occultation data. Forecasting Research Technical Report 471, Met Office, Exeter, UK.

Vorob'ev, V., and T. Krasil'nikova, 1994: Estimation of the accuracy of the atmospheric refractive index recovery from doppler shift measurements at frequencies used in the NAVSTAR system. *USSR Phys. Atmos. Ocean, Engl. Transl.*, **29**, 602–609.

Wickert, J., C. Reigber, G. Beyerle, R. König, C. Marquardt, T. Schmidt, L. Grunwaldt, R. Galas, T. Meehan, W. Melbourne, and K. Hocke, 2001: Atmosphere sounding by GPS radio occultation: First results from CHAMP. *Geophys. Res. Lett.*, **28**, 3263–3266.

Zou, X., H. Liu, R. Anthes, H. Shao, J. Chang, and Y.-J. Zhu, 2004: Impact of CHAMP radio occultation observations on global analyses and forecasts in the absence of AMSU radiance data. *J. Met. Soc. Jap.*, **82**, 533–549.